A Novel Tumor-Microenvironment Model that Combines Bioprinting and Tissue Culture to Investigate Cancer Cell and Microvascular Interactions

Ariana D. Suarez-Martinez^a, Marc Sole-Gras^b, Samantha S. Dykes^c, Zachary R. Wakefield^c, Kevin Bauer^a, Dima Majbour^a, Angela Bundy^c, Christine Pampo^c, Matthew E. Burow^d, Dietmar W. Siemann^c, Yong Huang^b, Walter L. Murfee^{a,*}

a J. Crayton Pruitt Family Department of Biomedical Engineering, University of Florida, Gainesville, FL 32611, USA

b Department of Mechanical and Aerospace Engineering, University of Florida, Gainesville, FL 32611, USA

c Department of Radiation Oncology, University of Florida, Gainesville, FL 32611, USA

d Department of Medicine, Tulane University, New Orleans, LA 70118, USA

*Corresponding Author: Walter Lee Murfee

Permanent Address: J. Crayton Pruitt Family Department of Biomedical Engineering

University of Florida

Biomedical Sciences Building, J284

1275 Center Dr. Gainesville, FL 32611 Phone: (352) 294-8813 Fax: (352) 273-9221

Email: wmurfee@bme.ufl.edu

ABSTRACT

A challenge in cancer research is the lack of physiologically responsive in vitro models that enable tracking of cancer cells in tissue-like environments. A model that enables real-time investigation of cancer cell migration, fate, and function during angiogenesis does not exist. Current models, such as 2D or 3D in vitro culturing, can contain multiple cell types, but they do not incorporate the complexity of intact microvascular networks. The objective of this study was to establish a tumor-microvasculature model by demonstrating the feasibility of bioprinting cancer cells onto excised mouse tissue. Inkjet-printed Dil+ breast cancer cells on mesometrium tissues from C57Bl/6 mice demonstrated cancer cells' motility and proliferation via time-lapse imaging. Co-localization of DAPI+ nuclei confirmed that DiI+ cancer cells remained intact postprinting. Printed Dil+ 4T1 cells also remained viable after printing on Day 0 and after culture on Day 5. Time-lapse imaging over 5 days enabled tracking of cell migration and proliferation. The number of cells and cell area were significantly increased over time. After culture, cancer cell clusters were co-localized with angiogenic microvessels. The number of vascular islands, defined as disconnected endothelial cell segments, was increased for tissues with bioprinted cancer cells, which suggests that the early stages of angiogenesis were influenced by the presence of cancer cells. Bioprinting cathepsin L knock-down 4T1 cancer cells on wild-type tissues or non-target 4T1 cells on NG2 knock-out tissues served to validate the use of the model for probing tumor cell versus microenvironment changes. These results establish the potential for bioprinting cancer cells onto live mouse tissues to investigate cancer-microvascular dynamics within a physiologically relevant microenvironment.

Key Words: Tumor Microenvironment, Bioprinting, Inkjet Printing, Cell Printing, Tissue Culture, Intact Microvasculature, Angiogenesis, Multicellular-Microvascular Interactions, Multicellular System, Micro-Physiological System, Cancer Cell Dynamics, Breast Cancer Cells

INTRODUCTION

Cancer represents a significant challenge to public health in the United States and worldwide and an opportunity for the biomedical engineering field. Solid tumors account for the majority of cancer-related deaths¹, yet drug attrition rates remain high for the treatment of these diseases^{2,3}. One potential explanation for these high attrition rates is the lack of *in vitro* tumor microenvironment models at the preclinical level. In addition to neoplastic cells, solid tumors are comprised of many host cell types within the tumor microenvironment.⁴ It is increasingly clear that neoplastic cells influence host cells to promote angiogenesis, growth, metastasis, drug resistance, and other tumorigenic phenotypes.⁵ Tumor-associated host cells and their interactions with neoplastic cells offer attractive therapeutic targets for their key roles in tumor progression.⁶ Therefore, understanding of these cancer cell dynamics and cell-environment interactions are crucial for the development of new therapeutic modalities. However, the challenge is the lack of models that mimic the complexity of the *in vivo* environment while still enabling the control to probe specific cell and environmental alterations.

To meet this challenge, tissue engineering has focused on the development of biomimetic models that incorporate *in vitro* cell assays, microfluidics, and bioprinting. Advances in these bottom-up approaches are highlighted, for example, by 3-dimensional microfluidic models which have a higher complexity compared to 2- and 3-dimensional *in vitro* assays. Microfluidic devices typically have multiple cell types, patterned channels, fluid flow and an extracellular matrix.⁷ These microfluidic approaches are being used for the investigation of tumor cell migration dynamics^{8,9}, the effects of hypoxia on extravasation¹⁰, and effects of environmental gradients on tumor cells¹¹. Another emergent technology is 3-dimensional bioprinting.¹² Three-dimensional printing of complex, functional living tissues is made feasible due to the widespread use of additive manufacturing technologies with biocompatible and cell-laden biomaterials.¹³⁻¹⁵ A recent study has 3-dimensional printed a scaffold-free tumor

containing fibroblasts, cancer cells and endothelial cells that arrange themselves similar to *in vivo* tumors. ¹⁶ Another study has focused on creating vascularized-oriented models by bioprinting a perfused channel lined with endothelial cells that is adjacent to a cluster of glioma stem cells in order to study glioblastoma-vascular dynamics. ¹⁷

Despite the advancements of these bottom-up engineered models and the demonstration of their usefulness for cancer research, the goal to recapitulate in vivo complexity motivates new approaches that intersect engineering and physiology. The objective of this study is to develop a novel in vitro tumor microenvironment in vitro model containing microvascular networks by incorporating bioprinting methodology and a recently introduced ex vivo mouse tissue culture model. We introduce the potential for bioprinting on live, mouse tissues. This topdown approach to spatially control the addition of cells to an intact tissue expands the potential applications of bioprinting and showcases a model for modulating cell and microenvironment interactions, independently. The mesometrium is a thin, translucent connective tissue that is easily harvested, self-contained, and maintained in culture. 18 Its simplicity and the fact that it contains intact microvasculature make this mouse tissue ideal for bioprinting exogenous cancer cells to be able to investigate cancer and microvascular dynamics. In this study, we demonstrated that exogenous breast cancer cells were successfully bioprinted in a pattern onto live, mouse tissue that contained intact microvascular networks. The bioprinted cancer cells and the tissue remained viable during ex vivo culture for 5 days. Time-lapse imaging allowed the tracking of cancer cells which revealed their proliferative and migratory dynamics within an intact microvasculature. Furthermore, studies with genetically modified breast cancer cells and genetically modified tissues demonstrated the ability to probe neoplastic cancer cell and host microenvironment changes. Cancer cell patterning over an explanted murine tissue and timelapse imaging introduce a new experimental platform for investigating cancer cell migration and effects on angiogenesis.

MATERIALS AND METHODS

Culturing and Labeling Cells

The breast cancer cell lines used in these experiments were 4T1 murine cells obtained from American Type Culture Collection (Manassas, VA, USA). Cells were cultured in RPMI media supplemented with 10% fetal bovine serum (FBS) and maintained under normal culture conditions (37°C and 5% CO₂). Cells were subcultured upon reaching 75% confluence. Nontarget (NT: SHC202V) and cathepsin L knock-down (CTSL KD: TRCN0000030580) cells were generated using Sigma Mission Lentiviral Particles (Sigma Aldrich, St. Louis, MO, USA). NT and KD cells were maintained under normal culture conditions in the presence of 3 µg/mL puromycin. For bioprinting, 15 million cells were labeled with Vybrant CM-Dil (Molecular Probes, Eugene, OR, USA) as per manufacturer's protocol. Briefly, cells in suspension were centrifuged at 600 G for 5 minutes and then resuspended with 4 mL of minimum essential media (MEM; Gibco, ThermoFisher Scientific, Waltman, MA, USA) + 1% Penicillin-Streptomycin (Pen-Strep; Gibco, ThermoFisher Scientific, Waltman, MA, USA) containing 20 μL of the Dil solution. The cells were then incubated at 37°C for 5 minutes following another incubation at 4°C for 15 minutes. They were centrifuged again at 600 G for 5 minutes to be washed one time with Dulbecco's phosphate buffered saline (DPBS; Gibco, ThermoFisher Scientific, Waltman, MA, USA) before being resuspended in 600 μL of MEM + 1% Pen-Strep supplemented with 10% FBS.

Transwell Assay

Transwell inserts (8 μ m pore) were coated with 50 μ L 1:5 dilution of Matrigel:RPMI, respectively. Inserts were then incubated at 37°C for 30 minutes to allow the Matrigel to solidify. Complete medium was added to the underside of the insert and 10⁴ 4T1 cells were suspended in 200 μ L

serum free RPMI and plated on top of the solidified Matrigel. Cells were allowed to invade through the Matrigel for 24 hours at 37 °C and 5% CO_2 , then fixed with 70% ethanol and stained with 0.1% crystal violet. Any cells and Matrigel remaining on the top of the insert were removed with a cotton swab. Cells that invaded to the underside of the insert were counted, n = 4.

Cell Proliferation Assays

For *in vitro* cells: In a 96-well plate, 4T1 cells were seeded at 10^3 cells/well in a total volume of $100 \,\mu$ L complete media. Cells were grown at 37° C in 5% CO₂. Cells were incubated with $10 \,\mu$ L of Cell Counting Kit-8 (CCK8-Dojindo Molecular Technologies, Rockville, MD, USA) reagent for one hour at 37° C. Cell proliferation was assessed by measuring the absorbance at $450 \, \text{nm}$, n = 3.

For bioprinted cells: After 3 days of culture, mesometrium tissues with printed cancer cells were labeled for BrdU, E-Cadherin and DAPI. Briefly, BrdU (Sigma Aldrich, St. Louis, MO, USA) dissolved in MEM + 1% Pen-Strep (1 mg/mL) was added to each well after removing old media and incubated under normal culture conditions for 2 hours. Tissues were then spread on microscope slides and fixed in 4% paraformaldehyde for 10 minutes at room temperature. After 3, 10-minute washes with PBS, they were placed in a 2M hydrochloric acid solution for 1 hour at 37°C. Following another three, 10-minute washes with PBS + 0.1% saponin, tissues were labeled with polyclonal rabbit anti-brdU (Abcam, Cambridge, MA, USA) primary antibody diluted at 1:100 with PBS + 0.1% saponin + 2% bovine serum albumin (BSA) + 5% normal goat serum (NGS) incubated at 4°C overnight. The next day, following three, 10-minute washes with PBS + 0.1% saponin, tissues were incubated with the secondary antibody, goat anti-rabbit Alexa Fluor-594 (Jackson ImmunoResearch Laboratories, West Grove, PA, USA), diluted at 1:100 with PBS + 0.1% saponin + 2% BSA + 5% NGS incubated at room temperature for 1 hour in the dark. After washing, they were labeled with FITC-conjugated E-Cadherin (BD Biosciences, San Jose, CA, USA) diluted at 1:100 with PBS + 0.1% saponin + 2% BSA + 5% NGS incubated at room

temperature for 1 hour in the dark. Following washes, tissues were labeled with DAPI

(ThermoFisher Scientific, Waltham, MA, USA) stain diluted at 1:3000 with PBS + 0.1% saponin

+ 2% BSA incubated at room temperature for 10 minutes in the dark.

Immunoblot

Whole cell lysates were harvested in RIPA buffer supplemented with protease inhibitor (Sigma Aldrich, St. Louis, MO, USA). Lysates were incubated on ice for 30 minutes with periodic vortexing prior to centrifugation at 10,000 RPM at 4°C. Protein concentration was normalized using BCA assay and equal concentration of proteins were diluted in Laemmli Buffer (0.125M Tris, 4% SDS, 20% glycerol, β-mercaptoethanol) and boiled for 5 minutes. Lysates were run on a polyacrylamide gel and transferred to PVDF membrane prior to blocking in 5% milk in TBST (20mM Tris, 137mM NaCl, 0.1% Tween 20, pH 7.5) for 1 hour. Primary antibodies utilized were against cathepsin L (R&D Systems, Minneapolis, MN, USA) and actin (Sigma Aldrich, St. Louis, MO, USA) used at 1:2,000 and 1:20,000, respectively. Primary antibodies were incubated in 5% bovine serum albumin (BSA) in TBST overnight at 4°C. HRP-conjugated secondary antibodies were incubated for at least 1 hour in TBST followed by detection using the Pierce ECL2 reagent (ThermoFisher Scientific, Waltham, MA, USA).

Animal Models

All animal experiments were approved by University of Florida's Institutional Animal and Care Use Committee. Six to eight week-old female BALB/c mice were injected via tail vein with 10⁴ NT shRNA or CTSL shRNA expressing 4T1 cells in a total volume of 100 µL phosphate buffered saline (PBS). Three weeks after inoculation, mice were euthanized and their lungs were harvested. The number of macroscopic lung colonies were counted, n=10. For the mammary intraductal models, one year-old retired breeder female BALB/c mice were anesthetized using isoflurane and injected in their left 4th mammary with 10³ NT shRNA or CTSL shRNA expressing

4T1 cells in a total volume of 10 μ L. Mammary tumors were measured over time using calipers (Tumor volume = Length x width²). At humane endpoints, mice were euthanized and mammary tumors and lungs were harvested, n=14.

Mouse Mesometrium Tissue Harvesting

The protocol followed for tissue harvesting is from Suarez-Martinez et al. 2018. Briefly, 10 to 16 week-old, female C57BL/6, wild-type (WT) and neuron-glial antigen 2 knock-out (NG2 KO) mice were euthanized by CO₂ asphyxiation followed by cervical dislocation. The abdominal fur was removed and the abdomen was sterilized with 70% isopropyl and iodine. After cutting the abdominal skin and muscle and moving all the organs to expose the uterine horns, the mesometrium tissues were harvested. The mesometrium tissue is the connective tissue of the uterine horn in female mice. The excised tissues were rinsed in warm DPBS, transferred to warm MEM and 1% Pen-Strep, and then moved into the incubator set to normal culture conditions.

Inkjet Printing Breast Cancer Cells

In a biosafety cabinet, individual mesometrium tissues were spread on a polycarbonate filter fitted to a cell-crown insert (Sigma-Aldrich, St. Louis, MO, USA) and then placed on a 100 mm sterile petri dish. The dish with the tissue was then transferred out of the biosafety cabinet and on top of the stage of the inkjet bioprinter. The cell bioink used was comprised of Dil-positive breast cancer cells suspended in cell medium (MEM + 1% Pen-Strep + 10% FBS) and 2% (w/v) sodium-alginate (Acros Organics, NJ, USA) solution mixed in a 2:1 ratio, respectively. The cell bioink was deposited using drop-on-demand inkjet printing, as illustrated in Figure 1, for its accurate performance as described in previous studies. ^{19–21} Specifically, the cell bioink was deposited via droplets onto the mesometrium tissue using an inkjet system comprised by a 120 µm ABL piezoelectric printhead (MicroFab, Plano, TX, USA) whose control module generated

the voltage excitation waveform, an *xy* motorized motion stage (Aerotech, Pittsburgh, PA, USA) to adjust the position of the printhead, and a pneumatic controller (MicroFab, Plano, TX, USA) ensuring enough fluid back pressure to maintain proper menisci levels of the cell bioink. Herein the excitation waves used are described as follows: driving voltage of +/- 120 V, frequencies of 2 Hz, dwell/echo times of 40-45 µs, and rise and fall times of 8-10 µs. A single cancer cell spot per tissue was created, each containing 10-12 droplets of the cell bioink in the same location. Warm MEM + 1% PenStrep was added on top of the tissue about 30 seconds after printing and then incubated for 5 minutes under normal culture conditions. The tissue with cells was then inverted into a well of a 6-well culture plate with 1 mL of MEM + 1% PenStrep supplemented with 20% FBS; 3 mL more of the culture medium was added to have a total of 4 mL of MEM + 1% PenStrep + 20% FBS. The tissues with cells were then placed in an incubator set to normal culture conditions for up to 5 days, where the culture media were changed every 24 hours, n = 7 per group.

Quantification of Motility and Proliferation of Bioprinted Breast Cancer Cells

The spot of Dil-positive breast cancer cells (NT and CTSL KD) that were bioprinted onto the mesometrium tissues were imaged every 24 hours starting at Day 0 to create a time-lapse.

Utilizing ImageJ software, the motility and proliferation of the printed cells were quantified. For motility calculated on Day 0, 1, and 2, a perimeter was traced to enclose the spot of Dil-positive cells measured in mm². Motility on Day 5 was quantified from immunohistochemistry labeled tissues by tracing the perimeter of E-Cadherin-positive cells. All area measurements correspond to the pixel per mm ration that is determined by the objective used to create the image. For proliferation calculated on Day 0, 1, and 2, the Cell Count plugin was used to count the individual Dil-positive cells. Proliferation on Day 5 was quantified from immunohistochemistry labeled tissues by creating a rectangle within the drawn perimeter enclosing all the E-Cadherin-positive cells. The area of the rectangle was the equivalent of 5% of the total cell area. The Cell

Count plugin was then utilized to count the E-Cadherin-positive cells within the drawn rectangle containing an area that is representative of the total cell area. The total number of cancer cells on Day 5 that correlates to proliferation is calculated by multiplying the number of cells counted in the rectangle by 20.

Quantification of Angiogenesis from Mesometrium Tissues with Bioprinted Breast Cancer Cells

ImageJ was used to quantify the microvascular remodeling of mesometrium tissues that had bioprinted breast cancer cells after 5-day ex vivo culture. This quantification analysis was blinded. Montages of whole tissues allowed to quantify the total number of sprouts, segments and vascular islands of the entire tissue. The obtained numbers were normalized with the total vascular length. These numbers were obtained using the Cell Count plug-in while the length was measured using the segmented line to trace all the vasculature. The ratio of pixel per mm, according to the camera and objective, was applied to the images to acquire the correct vascular length. To ensure consistency and reproducibility while analyzing data, we clearly defined all that was quantified. A sprout was defined as a blind-ended segment with only one side being connected to the network. A segment was defined as a connection between two nodes where sprouts were not counted as segments but vascular islands were counted as a segment. A vascular island was defined as disconnected segments that are not part of the main microvascular network, which could contain sprouts. Finally, vascular length was defined as the length of all microvascular networks that excluded sprouts but included vascular islands.

Immunohistochemistry

Mouse mesometrium tissues were spread on microscope slides to be fixed in 100% methanol at -20°C for 30 minutes and then washed 3 times with cold PBS + 0.1% saponin for 10 minutes each wash. The fixed tissues were then labeled with the following antibodies: 1:200 rat anti-

mouse platelet endothelial cell adhesion molecule (PECAM; BD Biosciences, San Jose, CA, USA) with 1:500 streptavidin-CY3 (Strep-CY3; Jackson ImmunoResearch Laboratories, West Grove, PA, USA) secondary, and 1:100 FITC-conjugated E-Cadherin (E-Cadherin; BD Biosciences, San Jose, CA, USA). All antibodies were diluted in antibody buffer solution which contained PBS + 0.1% saponin + 2% BSA + 5% NGS. All primary and secondary antibodies were incubated for 1 hour at room temperature in the dark. After every antibody incubation, tissues were rinsed three times with cold PBS + 0.1% saponin for 10 minutes.

Microscopy

Images were taken with a 4x, 10x, and 20x oil objectives from an inverted microscope, Nikon Eclipse Ti2, paired with an Andor Zyla camera. Time-lapse images of the Dil-positive cells during culture were imaged with a 4x and 10x objective. Whole tissue images with PECAM and E-Cadherin labeling were acquired with a 10x objective to extrapolate cancer cell motility and proliferation along with microvascular remodeling.

Statistical Analysis

Data are presented as mean ± standard error of mean (SEM). Proliferation and motility of cancer cells were compared across different culture days with repeated measures one-way Analysis of Variance (ANOVA) followed by Tukey's multiple comparisons tests to notify differences between the days. Proliferation and motility of cancer cells were compared across experimental groups (NT vs. Cathepsin L KD, WT vs. NG2 KO) with multiple unpaired two-tailed Student *t*-tests with Holm-Sidak correction to notify the differences between the groups per culture day. Angiogenesis and cathepsin L knock-down *in vitro* and *in vivo* data were compared using unpaired two-tailed Student *t*-tests with Welch's correction. A p-value < 0.05 was considered statistically significant. All the statistical analyses were executed using GraphPad Prism version 8.4 software.

RESULTS

Bioprinted Cancer Cells on Live Tissue is Viable and Reproducible

Murine 4T1 breast cancer cells were bioprinted onto a live mouse mesometrium tissue via an inkjet printer that contained the cell bioink reservoir to precisely deposit 10-12 cell droplets on the middle of the tissue. A schematic of the inkjet printer setup with the different elements needed for this novel protocol is shown in Figure 1. Bioprinted cancer cells that were pre-labeled with Dil revealed a circular spot of the exogenous cancer cells that adhered onto a certain predefined location of the tissue (Figure 2A). Time-lapse imaging demonstrated the ability to observe the proliferation and motility of the bioprinted Dil-positive cancer cells during 5 days in ex vivo culture (Figure 2A-F). A LIVE assay confirmed the viability of the bioprinted cancer cells immediately after printing (Figure 2G-I) and after 5 days in ex vivo culture (Figure 2J-L). Dil-positive cancer cells co-localized with DAPI-positive nuclei post printing further corroborating the success of cell deposition (Figure 2M-N). Moreover, the positive BrdU labeling after 3 days of ex vivo culture confirmed cancer cell proliferation (Figure 2O-R). E-cadherin antibody identified cancer cell clusters after 3 days (Figure 20). All E-cadherin-positive cancer cells had DAPI-positive nuclei, and a portion of the cells were also BrdU-positive (Figure 2R). The quantifications for the proliferation and motility of breast cancer cells were analyzed by counting the number of cells (Figure 2S) and measuring the cell area (Figure 2T), respectively. Repeated-measures one-way ANOVA revealed a significant difference between all days for the number of cells (Day 0: 159 \pm 41, Day 1: 370 \pm 78, Day 2: 889 \pm 184, Day 5: 18,031 \pm 1,696; p < 0.05; n = 7) and the cell area (Day 0: 0.72 ± 0.19 mm², Day 1: 1.89 ± 0.33 mm², Day 2: 2.92 ± 0.05 0.44 mm², Day 5: 5.93 ± 0.75 mm²; p < 0.05; n = 7) confirming the proliferation and motility of the bioprinted cancer cells on the mesometrium tissue. Hence, the data from Figure 2 validate

that the exogenous cancer cells that are bioprinted onto live mouse tissues remain viable, are proliferative and migrate away from their initial position.

Cathepsin L is Important for Invasion and Tumor Progression in Cancer

Previous studies have identified cathepsin L as a major regulator of the metastatic phenotype. Previous Studies to Validate the functional effects of inhibiting cathepsin L expression in cancer cells. With this rational, murine 4T1 breast cancer cells that stably express either non-target or cathepsin L shRNA were generated. Immunoblot of whole cell lysates revealed that cathepsin L was successfully knock-down using an independent cathepsin L-targeting shRNA compared to the non-target control (Figure 3A). Under normal *in vitro* culture conditions, cathepsin L knock-down cells proliferate at the same rate (Figure 3B; Day 1: NT 0.20 \pm 0.01, Cathepsin L KD 0.20 \pm 0.01, p = 0.1; Day 2: NT 0.26 \pm 0.03, Cathepsin L KD 0.27 \pm 0.03, p = 0.8; Day 3: NT 0.39 \pm 0.06, Cathepsin L KD 0.52 \pm 0.03, p = 0.1; n = 3). When assayed for their ability to invade through Matrigel in a transwell invasion assay, cathepsin L knock-down cells were significantly less invasive than the non-target shRNA expressing controls (Figure 3C; NT 92.5 \pm 14.1, Cathepsin KD 41.7 \pm 8.7, p = 0.038, n = 4). Together, these data suggest that cathepsin L is important for invasion, but not for *in vitro* proliferation.

The role of cathepsin L on the metastatic phenotype was also confirmed *in vivo* using the syngeneic BALB/c mammary intraductal (MIND) model. Briefly, 10^3 4T1 cells expressing non-target or cathepsin L shRNA were implanted into the left 4th mammary duct and tumor growth was measured over time using calipers. Cathepsin L knock-down resulted in tumors that took longer to initiate (Figure 3D; NT 19 ± 1 days, n = 14, Cathepsin KD 22 ± 1 days, n = 13, p = 0.029) and a longer time to reach humane endpoints (Figure 3E; NT 26 ± 1 days, n = 14, Cathepsin KD 30 ± 1 days, n = 13, p = 0.005) compared to the non-target shRNA expressing

tumors. Murine 4T1 cells are known to spontaneously metastasize to the lungs. As cathepsins are known to be involved in regulating multiple aspects of the metastatic cascade, we also assessed mice for spontaneous lung metastasis using the MIND model. Non-target and cathepsin L shRNA expressing 4T1 cells were injected into female BALB/c mice via the tail vein. Three weeks later, lungs were harvested and the number of visible tumor colonies were counted. Cathepsin L knock-down resulted in reduced number of lung nodules in this metastasis model (Figure 3F; NT 66.8 ± 4.5 , Cathepsin KD 23.7 ± 2.2 , p < 0.0001, n = 10).

Bioprinted Cathepsin L Knock-Down Cancer Cells on Intact Microvasculature Have Decreased Proliferation and Motility

Since cathepsin L has been shown to have an effect on tumor progression and metastasis, we tested the impact of cathepsin L during $ex\ vivo$ culture when murine 4T1 cathepsin L knock-down breast cancer cells were bioprinted on a tissue containing intact microvasculature in its native physiology. Dil-positive non-target (Figure 4A-C) and cathepsin L knock-down (Figure 4D-F) cancer cells were bioprinted on mesometrium tissues and time-lapsed to assess the proliferation and motility of the two types of cells on a microenvironment that has microvascular networks. The quantification for the number of cells (Figure 4G) and cell area (Figure 4H) during the different time points of $ex\ vivo$ culture were significantly different between the two groups after Day 1. Non-target and cathepsin L knock-down groups were significantly different on Day 2 and Day 5 for the number of cells (Day 2: NT 889 \pm 184, Cathepsin L KD 309 \pm 42, p = 0.028; Day 5: NT 18,031 \pm 1,696, Cathepsin L KD 7,060 \pm 1,043, p = 0.0005; n = 7) and the cell area (Day 2: NT 2.92 \pm 0.44 mm², Cathepsin L KD 1.46 \pm 0.21 mm², p = 0.033; Day 5: NT 5.93 \pm 0.75 mm², Cathepsin L KD 2.42 \pm 0.45 mm², p = 0.008; n = 7). The data suggest that cathepsin L knock-down cancer cells have a decreased proliferation

and motility compared to non-target cells when cultured after 1 day in a physiologically relevant ex vivo tissue.

Bioprinted Cancer Cells on NG2 Knock-Out Tissue with Intact Microvasculature Have Decreased Proliferation and Motility

To demonstrate the applicability of the model for investigating the effect of microenvironment alterations on cancer cell dynamics, we bioprinted murine 4T1 breast cancer cells on mesometrium tissues from wild-type (Figure 5A-C) or NG2 knock-out (Figure 5D-F) mice. Time-lapse images of the Dil-positive cancer cells bioprinted on both tissue types were analyzed to identify any changes in the proliferation or motility of the cancer cells. The quantification for the number of cells (Figure 5G) of both types of tissues during the different time points of ex vivo culture was significantly different after Day 1 (Day 2: WT 889 \pm 184, NG2 KO 448 \pm 76, p = 0.047; Day 5: WT 18,031 \pm 1,696, NG2 KO 12,994 \pm 2,252, p = 0.049; n = 7). Moreover, the quantification for the cell area (Figure 5H) of both types of tissues were significantly different after Day 0 (Day 1: WT 1.89 \pm 0.33 mm², NG2 KO 0.93 \pm 0.16 mm², p = 0.049; Day 2: WT 2.92 \pm 0.44 mm², NG2 KO 1.44 \pm 0.30 mm², p = 0.049; Day 5: WT 5.93 \pm 0.75 mm², NG2 KO 2.28 \pm 0.39 mm², p = 0.004; n = 7). The data suggest that the lack of NG2 expression by cells in the host microenvironment influenced cancer cell proliferation and motility compared to a wild-type tissue microenvironment.

Bioprinted Cancer Cells Have an Effect on the Early Stages of the Angiogenic Microvasculature

A key advantage of this platform is the ability to evaluate the spatial coordination and functional relationships between the exogenous, printed cancer cells and the microvasculature.

After 5 days in *ex vivo* culture, tissues that had bioprinted murine 4T1 breast cancer cells were

fixed and labeled with E-cadherin and PECAM to visualize the cancer cells and endothelial cells, respectively (Figure 6). Observation of the PECAM-positive blind-ended sprouts suggest that the native microvasculature in the mesometrium tissue was angiogenic (Figure 6A, 6D). Furthermore, E-cadherin-positive breast cancer cell clusters (Figure 6B, 6E) were observed to colocalize with high density PECAM-positive vessel regions, characteristic of an angiogenic response (Figure 6C, 6F). The changes in angiogenesis after a 5-day ex vivo culture were quantified by counting the number of sprouts, segments, and vascular islands from the sham control (Figure 7A-C) and the group with bioprinted breast cancer cells (Figure 7D-F). Although the presence of cancer cells did not appear to have a significant effect on the sprout density (Figure 7G; Sham 3.77 ± 0.36 #/mm, Cancer Cells 4.22 ± 0.35 #/mm, p = 0.38, n = 7), or the vascular density (Figure 7H; Sham 7.71 ± 0.93 #/mm, Cancer Cells 11.16 ± 1.37 #/mm, p = 0.061, n = 7), there was a significant increase in the vascular island density (Figure 7I; Sham 0.32 ± 0.08 #/mm, Cancer Cells 1.14 ± 0.31 #/mm, p = 0.036, n = 7) when compared to the sham control suggesting a differential effect on cancer cell presence on the angiogenic response to the culture conditions.

DISCUSSION

The novelty of the current study is the demonstration of cancer cell bioprinting on live, murine tissue enabling 1) the investigation of cancer cell migration in an intact, tissue environment, 2) the probing of cell versus microenvironment effects on cancer cell dynamics, and 3) the investigation of cancer cell aggregation on microvascular network growth. To our knowledge, this is the first tumor microenvironment model that incorporates exogenous cells onto live mouse tissue via inkjet printing to better recapitulate the complexity of real vascularized tissue.

Our study was inspired by the work of Phamduy *et al.* in 2015 who they laser direct-write printed breast cancer cells on live rat mesentery tissue.²⁶ The contribution of our study is the advancement of this approach utilizing a more common inkjet method and, more impactful, the use of murine tissue. The bioprinting on murine tissue now can be leveraged to expand the types of cell versus microenvironment cancer research related questions. To this end, we demonstrate the applications of the novel approach by probing the effect of cathepsin L knockdown in cancer cells and the effect of an altered tissue environment (i.e. tissues harvested from wild-type versus NG2 knock-out mice).

We foresee the potential that this novel methodology can have based on its real tissue microenvironment, precise incorporation of any kind of cell type, and ability to manipulate the host environment. Recently, biomimetic models are becoming common *in vitro* models for cancer research, such as microfluidic devices and bioprinting fabrication. Haessler *et al.* used a microfluidic device to highlight the impact that interstitial flow has on cancer cell migration responses from various breast cancer cell subpopulations. Intravasation and extravasation of tumor cells have also been investigated using microfluidic assays. Most recently, Kamm and colleagues developed a microfluidic comprised of 3-dimensional microvasculature to study how hypoxia affects the extravasation of breast cancer cells. Another recent study created a

microfluidic model to investigate the effects under various metabolic starvation gradients.¹¹

Utilizing bioprinting techniques to create biomimetic models for cancer research has also recently seen rapid advancements. Bioprinting has allowed the development of many different 3-dimensional cancer-type *in vitro* models like ovarian cancer²⁹, glioblastoma¹⁷, and breast cancer³⁰. Most recently, Langer *et al.* 3-dimensional bioprinted an architecturally defined, multicell, and scaffold-free tissue that recapitulated a human primary tumor that is capable of investigating heterogeneity in therapeutic response, signaling and migration.¹⁶

Our model aims to become an intermediate model between *in vitro*, 2-dimensional studies and *in vivo* studies. The mouse mesometrium culture model utilized in this study is an *ex vivo* model that has many beneficial characteristics and capabilities: 1) containing intact microvascular networks with identifiable arterioles, venules, and capillaries, 2) containing perivascular cells like smooth muscle cells and pericytes, 3) containing lymphatics, peripheral nerves, and immune cells, 4) time-lapse imaging, and 5) inducing angiogenesis. While it has great advantages, limitations of the study include the lack of perfusion in the microvessels which is known to regulate endothelial sprouting. Teture experiments are necessary to incorporate this feature, although this is a common limitation in widely used *in vitro* cancer cell models and *ex vivo* angiogenic models like retina explant and aortic ring assays that have advanced microvascular dynamics knowledge. Another limitation is the lack of real tumor-stroma microenvironment since the mesometrium tissue is from healthy, cancer-free mice. Future experiments are needed to observe long term cancer cell dynamics that would show the ability of the bioprinted cancer cells to form tumors.

For accurate deposition of cell bioinks, the droplet-on-demand (DOD) dispensing mechanism systems are generally preferred to produce finer features with better resolution than others based on extrusion methods.³⁴ The main DOD bioprinting approaches include laser-induced forward transfer (LIFT)^{35–37} and inkjetting^{19,21,38}. While LIFT enables the deposition of highly viscous inks given its orifice-free nature, the droplet formation process is generally

difficult to be controlled precisely.³⁹ Therefore, to obtain repetitive and accurate deposition results, inkjet printing was chosen for this study; a simple schematic of the methodology is shown in Figure 1. Since inkiet printing is preferred for low-viscosity inks, the bioink utilized in this study was a low-concentration of alginate-based cell bioink. The ink was carefully chosen because the rheological properties of the deposited cell bioink are crucial factors that determine the extent of the spreading degree of the deposited material on the receiving substrate. As such, sodium alginate, a widely utilized biomaterial⁴⁰, was chosen as a biocompatible rheology modifier to increase the viscosity of the ink ensuring a good post-printing pattern preservation. Specifically, a final concentration of approximately 0.7 % (w/v) of sodium alginate in the cell bioink was used which helped preserve the printed droplet pattern after the addition of media to the tissue while maintaining good jetting performance of the bioink. Additionally, the incorporated exogenous cells were still able to migrate and proliferate under the presence of this low-concentration alginate solution. The issue of the bioink is an important one, as initial trials with a lower viscosity media resulted in lack of patterning control due to fluid dispersion over the tissue (data not shown). Hence, while our results demonstrate the successful adoption of inkjet printing in this study future studies are needed to compare the effects of other bioink options.

By inkjet printing the 4T1 breast cancer cells, we successfully deposited the exogenous cells in a circular pattern onto the mouse mesometrium tissue (Figure 2A). Murine 4T1 breast cancer cells were utilized for these experiments because this is an aggressive mammary carcinoma cell line that is highly invasive and tumorigenic.⁴¹ These characteristics enable the 4T1 cells to undergo the printing process with ease due to their resilience and to be easily incorporated into the tissue. Performing a LIVE assay and showing DAPI-positive nucleated cells, demonstrate that cancer cells remain viable (Figure 2G-I) and intact (Figure 2M, N) after the printing protocol. To further corroborate their viability, cells were labeled with Dil prior to printing to allow for short-term tracking via time-lapse imaging every 24 hours. Although it was

observed that the cells were migratory and proliferative during ex vivo culture for 5 days (Figure 2A-F), only time-lapse data from Day 0 until Day 2 were analyzed to quantify the number of cells (Figure 2S) and cell area (Figure 2T) that correspond to proliferation and migration, respectively. The reason being, that the particular labeling agent used, Dil, is incorporated into the cytoplasm of each cell which results in a decreased expression when the cells divide and proliferate. As the cells undergo mitosis, the daughter cells are only able to express half of the Dil-label compared to their parental cell and after 7 generations the Dil is no longer observable. Due to this limitation and to prevent unreliable data, time-lapse images after Day 2 were not quantified. However, proliferation and migration were quantified after 5 days in culture, by fixing and labeling tissues with E-cadherin to identify the cancer cells. Since E-cadherin labels the adherens junctions between epithelial cells that form clusters⁴², bioprinted Dil-positive cancer cells on Day 0 do not label for E-cadherin (data not shown). In this ex vivo mouse tissue model, the expression of E-cadherin from cancer cells begins on Day 2, where we observed very small clusters, less than 10 cells (data not shown). On Day 3, the E-cadherin-positive clusters are larger (Figure 2O), indicating that as time progresses cancer cells begin to express more Ecadherin until large clusters are observed on Day 5.

Bioprinting cathepsin L knock-down cancer cells on wild-type mesometrium tissue supports the use of our model for probing the effects of manipulating the cell type. Cathepsin L was selected as the target molecule because the cysteine cathepsin family of proteases have been proven to be implicated in cancer progression, metastasis, invasion and proliferation (review in ref. ⁴³). More specifically, cathepsin L has been shown to be upregulated in various malignant cancers such as breast, lung, and gastric carcinomas, melanomas and gliomas. ^{44–47} The expression levels of cathepsin L have revealed a positive correlation with the grade of cancer malignancy and prognosis. ^{48,49} For our study, cathepsin L knock-down 4T1 breast cancer cells were engineered and immunoblot confirmed the decreased of cathepsin L expression (Figure 3A). *In vitro* testing confirmed that cathepsin L knock-down decreased cell

invasion (Figure 3C) but not proliferation (Figure 3B) which is consistent with current literature. ^{23,50} *In vivo* experiments demonstrated that cathepsin L knock-down impaired tumor progression (Figure 3D-E) and metastasis (Figure 3F) which also corroborated prior findings. ⁵¹ Other *in vivo* experiments also demonstrated that cathepsin L knock-down decreased tumor mass (data not shown) suggesting an effect on *in vivo* proliferation which is consistent with a study by Gocheva *et al.* This study showed that cathepsin L knock-out mice had decreased cell proliferation in tumors assessed with BrdU labeling. ⁵¹ When cathepsin L knock-down cancer cells were bioprinted onto an *ex vivo* tissue containing intact microvasculature with native physiology, the number of cells (Figure 4G) and the cell area (Figure 4H) was significantly decreased compared to non-target on Day 2 and 5. Interestingly, this validates the use of our model for evaluating cathepsin L knock-down effects and more broadly for using the model to probe cell changes. Also, the effects of cathepsin knock-down on cell proliferation compared to the cell-based *in vitro* assay suggest that our results might be more reflective of the complex *in vivo* environment.

To establish the use of our model for evaluating microenvironment changes, we bioprinted 4T1 cancer cells onto neuron-glial antigen 2 (NG2) knock-out mesometrium tissues. NG2, also known as chondroitin sulfate proteoglycan-4 or melanoma chondroitin sulfate proteoglycan, is a surface type I transmembrane proteoglycan that has functional extracellular and intracellular domains which can activate important signaling pathways in cell migration, survival and angiogenesis. NG2 is expressed in a myriad type of cells including, but not limited to, pericytes, smooth muscle cells, mesenchymal stem cells, osteoblasts, melanocytes, and macrophages (review in ref. ⁵²). Since the mesometrium tissue contains pericytes, smooth muscle cells, and macrophages¹⁸, a global ablation of NG2 could have an impact on cell-to-cell interactions between the host microenvironment and exogenous cells. In regards to cancer, some tumor cells express NG2 and NG2-related signaling has been demonstrated to play a key role in tumor progression of various cancers like brain⁵³, breast⁵⁴, and skin⁵⁵. In our model,

bioprinted cancer cells on NG2 knock-out tissue resulted in a significantly decreased proliferation on Day 2 and 5 (Figure 5G), and decreased migration on Day 1, 2, and 5 (Figure 5H). These results can be explained by understanding the impact of NG2 on the stromal tissue surrounding tumors. Stromal cells of solid tumors frequently express NG2. Stallcup and colleagues designed elegant studies to investigate the contribution of NG2-expressing pericytes and macrophages on the progression of brain tumors. Their results demonstrated that pericyteand macrophage-specific NG2 null mice had delayed brain tumor progression 10 days after receiving an injection of melanoma cells; there was an 87% decrease in tumor volume from macrophage-NG2 knock-out mice and 77% decrease from pericyte-NG2 knock-out mice compared to the control.⁵⁶ These results suggest that expression of NG2 in the microenvironment can be essential for normal cancer cell dynamics and the ablation of NG2 in the microenvironment would therefore negatively impact cancer cell proliferation and migration. While further studies are necessary to elucidate cell-specific roles of NG2 in the host microenvironment for our studies, our findings suggest that NG2 inhibition can a play a role in initial cancer cell migration dynamics and more broadly support our approach for similar mechanistic studies aimed at isolating microenvironmental contributions.

Since sustained angiogenesis is one of the hallmarks of cancer⁵⁷, we wanted to assess the effects of cancer cells on microvasculature remodeling after culture. After 5 days in *ex vivo* culture, PECAM and E-cadherin labeling identified capillary sprouts (Figure 6A, 6D) and clustering of cancer cells (Figure 6B, 6E), respectively. Capillary sprouts are defined as blindended, PECAM-positive segments that come off microvascular networks and are indicative of angiogenesis, which is the growth of new blood vessels from pre-existing microvessels.⁵⁸ Fluorescence imaging revealed examples of breast cancer cell clusters with the angiogenic microvasculature (Figure 6C, 6F). Based on a plethora of literature, it is now widely accepted that tumor cells disrupt the balance of pro- and anti-angiogenic signals to sustain the development of new blood vessels into the tumor to provide oxygen and nutrients (review in ref.

⁵⁹). In our model, although the angiogenic metrics analyzed (sprout and vascular density) were not significantly different between the two groups, there was a trend where the presence of cancer cells led to a higher mean sprout and vascular density (p = 0.06). Important details to consider regarding the interpretation of these data are the number of cancer cells, the culture media, and the timing of the evaluation. The number of printed cancer cells on Day 0 ranged from 25 to 353. Additional experiments will be needed to determine whether an increased number of cells affects the angiogenic response. Also, the culture media for the cancer cell and control groups contained serum, which is known to stimulate angiogenesis¹⁸. An alternative control group could have included bioprinted cancer cells in serum-free media. Despite these potential issues, the tissues with cancer cells displayed a significant increase in the number of vascular islands (Figure 7I). Vascular islands are defined as disconnected, PECAM-positive segments that are not part of the main microvascular networks. Taken together, the data support the observation of cancer cells with angiogenic microvasculature in a real-tissue microenvironment. This further suggests that the cancer cells are having an effect and motivates follow-up studies to characterize the cancer cell influence of various vessel types along a microvascular network.

Furthermore, this methodology can be applied to study different types of cancers under various conditions because our protocol preserves the structure and complexity of *in vivo* environments for modeling early stages of tumor development. Cathepsin L was shown here to be an important mediator of breast cancer metastatic phenotypes. However, any number of anticancer therapeutic targets can be assessed, either via genetic or pharmacologic manipulation. Likewise, cell characteristics from the host microenvironment can be evaluated as potential modulators of tumorigenic phenotypes. NG2 knock-out mesometrium was shown here to alter cancer cell dynamics after 1 day in culture. Further, mesometrium tissue from diverse genetically modified mouse models can be readily applied to this methodology. Also, the bioprinted tissues can be cultured under different conditions, such as hypoxia or different

conditioned-media. The mesometrium was utilized to study multicellular microvasculature dynamics, but it can also be useful to further study neoplastic cell interactions with host immune cells since the mesometrium also has resident, CD11b-posivite macrophages. Additionally, other types of tissues can potentially be incorporated into this methodology. It is also plausible that biopsied human tissue can be utilized for this methodology, although it was not attempted here. Moreover, due to the advantages of inkjet printing, we would also be able to bioprint more than one cell type on the same tissue to observe their interactions with each other and the host microenvironment. For example, it would allow us to evaluate how fibroblasts or immune cells impact cancer cell dynamics and microvascular remodeling.

CONCLUSIONS

The current study introduces a novel methodology at the intersection of tissue engineering and physiology. This new demonstration of bioprinting exogenous cancer cells onto intact murine tissue serves to expand bioprinting applications and offers a new perspective for biomimetic model development. Our results establish a novel methodology that combines inkjet printing and mouse mesometrium culture model to precisely incorporate a spot of breast cancer cells onto live, mouse tissue to investigate cancer cell dynamics and angiogenesis within an intact microvasculature during culture. This study corroborates the manipulation of different exogenous cells and different host microenvironments that impact cancer cell dynamics in a physiologically relevant tissue. This methodology motivates a new approach for delineating the effects of the microenvironment on cancer cells and vice versa.

AUTHOR CONTRIBUTIONS

SSD, DWS, WLM, and YH conceptualization. ADSM managed project. ADSM, MSG, ZRW, SSD, AB, and CP acquired data. ADSM and MSG optimized printing methodology. ADSM and SSD analyzed data. KB and DM validated data. ADSM, MSG, ZRW, and SSD wrote original manuscript. ADSM, MSG, ZRW, SSD, WLM, DWS, YH, and, MB reviewed and edited manuscript.

CONFLICTS OF INTEREST

All authors declare no conflict of interest.

ACKNOWLEDGEMENTS

This study was funded by NIH R01AG049821 awarded to WLM, by NSF CMMI-1634755 awarded to YH, by Thomas H Maren Postdoctoral Fellowship awarded to SSD, and by NIH R01CA197477 awarded to DWS. The initial inkjetting printing support from Shinichi Sakurada is highly appreciated.

REFERENCES

- 1 Siegel RL, Miller KD, Jemal A. Cancer statistics, 2020. CA Cancer J Clin 2020; 70: 7–30.
- 2 Hutchinson L, Kirk R. High drug attrition rates—where are we going wrong? *Nat Rev Clin Oncol* 2011; **8**: 189–190.
- 3 Nixon NA, Khan OF, Imam H, Tang PA, Monzon J, Li H *et al.* Drug development for breast, colorectal, and non-small cell lung cancers from 1979 to 2014. *Cancer* 2017; **123**: 4672–4679.
- 4 Bussard KM, Mutkus L, Stumpf K, Gomez-Manzano C, Marini FC. Tumor-associated stromal cells as key contributors to the tumor microenvironment. *Breast Cancer Res* 2016; **18**. doi:10.1186/s13058-016-0740-2.
- 5 Hanahan D, Weinberg RA. Hallmarks of Cancer: The Next Generation. Cell 2011; 144: 646–674.
- 6 Dykes SS, Hughes VS, Wiggins JM, Fasanya HO, Tanaka M, Siemann D. Stromal cells in breast cancer as a potential therapeutic target. *Oncotarget* 2018; **9**: 23761–23779.
- 7 Jiang K, Dong C, Xu Y, Wang L. Microfluidic-based biomimetic models for life science research. *RSC Adv* 2016; **6**: 26863–26873.
- 8 Zervantonakis IK, Hughes-Alford SK, Charest JL, Condeelis JS, Gertler FB, Kamm RD. Three-dimensional microfluidic model for tumor cell intravasation and endothelial barrier function. *Proc Natl Acad Sci* 2012; **109**: 13515–13520.
- 9 Haessler U, Teo JCM, Foretay D, Renaud P, Swartz MA. Migration dynamics of breast cancer cells in a tunable 3D interstitial flow chamber. *Integr Biol* 2012; **4**: 401–409.
- 10 Song J, Miermont A, Lim CT, Kamm RD. A 3D microvascular network model to study the impact of hypoxia on the extravasation potential of breast cell lines. *Sci Rep* 2018; **8**: 1–11.
- 11 Ayuso JM, Virumbrales-Munoz M, McMinn PH, Rehman S, Gomez I, Karim MR *et al.* Tumor-on-a-chip: a microfluidic model to study cell response to environmental gradients. *Lab Chip* 2019; **19**: 3461–3471.
- 12 Knowlton S, Onal S, Yu CH, Zhao JJ, Tasoglu S. Bioprinting for cancer research. *Trends Biotechnol* 2015; **33**: 504–513.
- 13 Murphy SV, Atala A. 3D bioprinting of tissues and organs. Nat Biotechnol 2014; 32: 773–785.
- 14 Huang Y, Leu MC, Mazumder J, Donmez A. Additive Manufacturing: Current State, Future Potential, Gaps and Needs, and Recommendations. *J Manuf Sci Eng* 2015; **137**. doi:10.1115/1.4028725.
- 15 Huang Y, Schmid SR. Additive Manufacturing for Health: State of the Art, Gaps and Needs, and Recommendations. *J Manuf Sci Eng* 2018; **140**. doi:10.1115/1.4040430.
- 16 Langer EM, Allen-Petersen BL, King SM, Kendsersky ND, Turnidge MA, Kuziel GM *et al.* Modeling Tumor Phenotypes In Vitro with Three-Dimensional Bioprinting. *Cell Rep* 2019; **26**: 608–623.

- 17 Lee VK, Guohao Dai, Hongyan Zou, Seung-Schik Yoo. Generation of 3-D glioblastoma-vascular niche using 3-D bioprinting. In: *2015 41st Annual Northeast Biomedical Engineering Conference (NEBEC)*. IEEE: Troy, NY, USA, 2015, pp 1–2.
- 18 Suarez-Martinez AD, Bierschenk S, Huang K, Kaplan D, Bayer CL, Meadows SM *et al.* A Novel ex vivo Mouse Mesometrium Culture Model for Investigating Angiogenesis in Microvascular Networks. *J Vasc Res* 2018; **55**: 125–135.
- 19 Xu C, Chai W, Huang Y, Markwald RR. Scaffold-free inkjet printing of three-dimensional zigzag cellular tubes. *Biotechnol Bioeng* 2012; **109**: 3152–3160.
- 20 Christensen K, Compaan A, Chai W, Xia G, Huang Y. In Situ Printing-then-Mixing for Biological Structure Fabrication Using Intersecting Jets. *ACS Biomater Sci Eng* 2017; **3**: 3687–3694.
- 21 Sakurada S, Sole-Gras M, Christensen K, Wallace DB, Huang Y. Liquid-absorbing system-assisted intersecting jets printing of soft structures from reactive biomaterials. *Addit Manuf* 2020; **31**: 100934.
- 22 Rozhin J, Wade RL, Honn KV, Sloane BF. Membrane-associated cathepsin L: A role in metastasis of melanomas. *Biochem Biophys Res Commun* 1989; **164**: 556–561.
- 23 Sudhan DR, Siemann DW. Cathepsin L inhibition by the small molecule KGP94 suppresses tumor microenvironment enhanced metastasis associated cell functions of prostate and breast cancer cells. *Clin Exp Metastasis* 2013; **30**: 891–902.
- 24 Zhang W, Wang S, Wang Q, Yang Z, Pan Z, Li L. Overexpression of cysteine cathepsin L is a marker of invasion and metastasis in ovarian cancer. *Oncol Rep* 2014; **31**: 1334–1342.
- 25 Pulaski BA, Ostrand-Rosenberg S. Reduction of Established Spontaneous Mammary Carcinoma following Immunotherapy with Major Histocompatibility Complex Class II and B7.1 Cell-based Tumor Vaccines. *Cancer Res* 1998; **58**: 1486–1493.
- 26 Phamduy TB, Sweat RS, Azimi MS, Burow ME, Murfee WL, Chrisey DB. Printing cancer cells into intact microvascular networks: a model for investigating cancer cell dynamics during angiogenesis. *Integr Biol* 2015; **7**: 1068–1078.
- 27 Riahi R, Yang YL, Kim H, Jiang L, Wong PK, Zohar Y. A microfluidic model for organ-specific extravasation of circulating tumor cells. *Biomicrofluidics* 2014; **8**: 024103.
- 28 Chen MB, Whisler JA, Fröse J, Yu C, Shin Y, Kamm RD. On-chip human microvasculature assay for visualization and quantification of tumor cell extravasation dynamics. *Nat Protoc* 2017; **12**: 865–880.
- 29 Xu F, Celli J, Rizvi I, Moon S, Hasan T, Demirci U. A three-dimensional in vitro ovarian cancer coculture model using a high-throughput cell patterning platform. *Biotechnol J* 2011; **6**: 204–212.
- 30 Ling K, Huang G, Liu J, Zhang X, Ma Y, Lu T *et al.* Bioprinting-Based High-Throughput Fabrication of Three-Dimensional MCF-7 Human Breast Cancer Cellular Spheroids. *Engineering* 2015; **1**: 269–274.

- 31 Song JW, Munn LL. Fluid forces control endothelial sprouting. *Proc Natl Acad Sci* 2011; **108**: 15342–15347.
- 32 Sawamiphak S, Ritter M, Acker-Palmer A. Preparation of retinal explant cultures to study ex vivo tip endothelial cell responses. *Nat Protoc* 2010; **5**: 1659–1665.
- 33 Nicosia RF, Ottinetti A. Growth of Microvessels in Serum-Free Matrix Culture of Rat Aorta. *Lab Invest* 1990; **63**: 115–122.
- 34 Zhang Z, Jin Y, Yin J, Xu C, Xiong R, Christensen K *et al.* Evaluation of bioink printability for bioprinting applications. *Appl Phys Rev* 2018; **5**: 041304.
- 35 Lin Y, Huang Y, Chrisey DB. Droplet formation in matrix-assisted pulsed-laser evaporation direct writing of glycerol-water solution. *J Appl Phys* 2009; **105**. doi:10.1063/1.3116724.
- 36 Xiong R, Zhang Z, Chai W, Huang Y, Chrisey DB. Freeform drop-on-demand laser printing of 3D alginate and cellular constructs. *Biofabrication* 2015; **7**: 045011.
- 37 Vinson BT, Phamduy TB, Shipman J, Riggs B, Strong AL, Sklare SC *et al.* Laser direct-write based fabrication of a spatially-defined, biomimetic construct as a potential model for breast cancer cell invasion into adipose tissue. *Biofabrication* 2017; **9**: 025013.
- 38 Christensen K, Xu C, Chai W, Zhang Z, Fu J, Huang Y. Freeform inkjet printing of cellular structures with bifurcations: Approach Freeform Fabrication of Bifurcated Cellular Structures by Using a Liquid Support-Based Inkjet Printing Approach. *Biotechnol Bioeng* 2015; **112**: 1047–1055.
- 39 Zhang Z, Xiong R, Mei R, Huang Y, Chrisey DB. Time-Resolved Imaging Study of Jetting Dynamics during Laser Printing of Viscoelastic Alginate Solutions. *Langmuir* 2015; **31**: 6447–6456.
- 40 Augst AD, Kong HJ, Mooney DJ. Alginate Hydrogels as Biomaterials. *Macromol Biosci* 2006; **6**: 623–633.
- 41 Pulaski BA, Ostrand-Rosenberg S. Mouse 4T1 Breast Tumor Model. *Curr Protoc Immunol* 2000; **39**. doi:10.1002/0471142735.im2002s39.
- 42 Rübsam M, Mertz AF, Kubo A, Marg S, Jüngst C, Goranci-Buzhala G *et al.* E-cadherin integrates mechanotransduction and EGFR signaling to control junctional tissue polarization and tight junction positioning. *Nat Commun* 2017; **8**: 1–16.
- 43 Olson OC, Joyce JA. Cysteine cathepsin proteases: regulators of cancer progression and therapeutic response. *Nat Rev Cancer* 2015; **15**: 712–729.
- 44 Castiglioni T, Merino MJ, Elsner B, Lah T, Sloane BF, Emmert-Buck MR. Immunohistochemical Analysis of Cathepsins D, B, and L in Human Breast Cancer. *Hum Pathol* 1994; **25**: 857–862.
- 45 Dohchin A, Suzuki J, Seki H, Masutani M, Shiroto H, Kawakami Y. Immunostained cathepsins B and L correlate with depth of invasion and different metastatic pathways in early stage gastric carcinoma. *Cancer* 2000; **89**: 482–487.

- 46 Kos J, Stabuc B, Schweiger A, Krasovec M, Cimerman N, Kopitar-Jerala N *et al.* Cathepsin B, H, and L and Their Inhibitors Stefin and Cystatin C in Sera of Melanoma Patients. *Clin Cancer Res* 1997; **3**: 1815–1822.
- 47 Jedeszko C, Sloane BF. Cysteine cathepsins in human cancer. Biol Chem 2004; 385: 1017–1027.
- 48 Skrzypczak M, Springwald A, Lattrich C, Häring J, Schüler S, Ortmann O *et al.* Expression of Cysteine Protease Cathepsin L is Increased in Endometrial Cancer and Correlates With Expression of Growth Regulatory Genes. *Cancer Invest* 2012; **30**: 398–403.
- 49 Thomssen C, Schmitt M, Goretzki L, Oppelt P, Pache L, Dettmar P *et al.* Prognostic Value of the Cysteine Proteases Cathepsin B and Cathepsin L in Human Breast Cancer. *Clin Cancer Res* 1995; **1**: 741–746.
- 50 Reinheckel T. The lysosomal cysteine protease cathepsin L regulates keratinocyte proliferation by control of growth factor recycling. *J Cell Sci* 2005; **118**: 3387–3395.
- 51 Gocheva V. Distinct roles for cysteine cathepsin genes in multistage tumorigenesis. *Genes Dev* 2006; **20**: 543–556.
- 52 Ampofo E, Schmitt BM, Menger MD, Laschke MW. The regulatory mechanisms of NG2/CSPG4 expression. *Cell Mol Biol Lett* 2017; **22**. doi:10.1186/s11658-017-0035-3.
- 53 Brekke C, Lundervold A, Enger PØ, Brekken C, Stålsett E, Pedersen TB *et al.* NG2 expression regulates vascular morphology and function in human brain tumours. *NeuroImage* 2006; **29**: 965–976.
- 54 Cooney CA, Jousheghany F, Yao-Borengasser A, Phanavanh B, Gomes T, Kieber-Emmons AM *et al.* Chondroitin sulfates play a major role in breast cancer metastasis: a role for CSPG4 and CHST11gene expression in forming surface P-selectin ligands in aggressive breast cancer cells. *Breast Cancer Res* 2011; **13**. doi:10.1186/bcr2895.
- 55 Wang J, Svendsen A, Kmiecik J, Immervoll H, Skaftnesmo KO, Planagumà J *et al.* Targeting the NG2/CSPG4 Proteoglycan Retards Tumour Growth and Angiogenesis in Preclinical Models of GBM and Melanoma. *PLoS ONE* 2011; **6**: e23062.
- 56 Yotsumoto F, You W-K, Cejudo-Martin P, Kucharova K, Sakimura K, Stallcup WB. NG2 proteoglycandependent recruitment of tumor macrophages promotes pericyte-endothelial cell interactions required for brain tumor vascularization. *Oncolmmunology* 2015; **4**: e1001204.
- 57 Hanahan D, Weinberg RA. The Hallmarks of Cancer. Cell 2000; 100: 57–70.
- 58 Carmeliet P. Angiogenesis in life, disease and medicine. Nature 2005; 438: 932–936.
- 59 Carmeliet P, Jain RK. Angiogenesis in cancer and other diseases. Nature 2000; 407: 249–257.

FIGURE LEGENDS

- **Fig. 1.** Schematic of bioprinting exogenous cells onto live, *ex vivo* tissue. The inkjet system is comprised of a 120 μm ABL piezoelectric printhead whose control module generates the voltage excitation waveform, an *xy* motorized motion stage that adjusts the position of the printhead, and a pneumatic pressure controller that ensures enough fluid-back pressure to maintain proper menisci levels of cell bioink. The cells were printed on top of the mesometrium tissue that is spread on a cell-crown insert and inside a 100 mm petri dish. The excitation waves used for this inkjet printing system are the following: driving voltage of +/- 120 V, frequencies of 2 Hz, dwell/echo times of 40-45 μs, and rise and fall times of 8-10 μs.
- **Fig. 2.** Bioprinting mouse breast cancer cells on live, mouse tissue is viable and reproducible. (A-F) Dil-positive cancer cells were inkjet printed in a circular pattern (dashed circle) and timelapse imaged for 5 consecutive days. The mesometrium tissue and the bioprinted cancer cells remained viable after printing on Day 0 (G-I), and after culture on Day 5 (J-L). (M, N) Cancer cells were also shown to be nucleated immediately after being bioprinted. (O-R) After 3 days in culture, nucleated cancer cells started to form clusters, express E-Cadherin, and be proliferative. Proliferation (S) and motility (T) of bioprinted cancer cells were quantified during *ex vivo* culture. Data is shown as the mean \pm SEM and * represents p < 0.05, n = 7. Scale bars = 500 μm (A-F), 250 μm (G-N), 50 μm (O-R).
- **Fig. 3.** Cathepsin L is not important for *in vitro* proliferation in 4T1 murine breast cancer cells but it is for *in vitro* invasion and *in vivo* tumor progression and metastasis. (A-C) *In vitro* experiments using 4T1 murine breast cancer cells indicated the importance of cathepsin L in invasion but not in cell proliferation. A) Whole cell lysates were analyzed by immunoblot. B) Cells were plated at

equal numbers and proliferation was assessed over time using the CCK8 reagent. C) Cells were plated on top of transwell inserts and allowed to invade through Matrigel for 24 hours. Cells were then fixed and stained with crystal violet and the number of invaded cells was counted. (D-F) *In vivo* experiments indicated the importance of cathepsin L in tumor progression and metastasis. Non-target, NT, shRNA or CTSL, KD, shRNA expressing cells were implanted in the mammary ducts of female BALB/c mice and D) the number of days from time of injection until tumors became palpable, and E) the number of days from injection until humane endpoints were reached were quantified. F) Non-target, NT, shRNA or CTSL, KD, shRNA expressing cells were injected via the tail vein of female BALB/c mice and the number of visible nodules per lung were quantified after three weeks. Data is shown as the mean ± SEM and *, **, *** represent p < 0.05, p < 0.002, p < 0.0001, respectively.

- **Fig. 4.** Cathepsin L knock-down in breast cancer cells decrease proliferation and motility during $ex\ vivo$ culture. Prelabeled Dil non-target, NT (A-C), or cathepsin L knock-down, KD (D-F), 4T1 murine breast cancer cells were bioprinted on mesometrium tissues containing intact microvasculature with its native physiology. Proliferation (G) and motility (H) of bioprinted non-target (black circle symbol) and cathepsin L knock-down (blue triangle symbol) cancer cells on mesometrium tissues were quantified during $ex\ vivo$ culture. Data is shown as the mean \pm SEM and * represents p < 0.05, n = 7. Scale bars = 500 μm.
- **Fig. 5.** Bioprinted breast cancer cells on NG2 knock-out tissues have decreased proliferation and motility during *ex vivo* culture. Prelabeled Dil 4T1 murine breast cancer cells were bioprinted on wild-type, WT (A-C), or neuron-glial antigen 2 knock-out, NG2 KO (D-F) mesometrium tissues containing intact microvasculature with its native physiology. Proliferation (G) and motility (H) of bioprinted 4T1 murine breast cancer cells on wild-type (black circle

symbol) and neuron-glial antigen 2 knock-out (purple triangle symbol) mesometrium tissues were quantified during *ex vivo* culture. Data is shown as the mean \pm SEM and * represents p < 0.05, n = 7. Scale bars = 500 μ m.

Fig. 6. Breast cancer cells colocalize with the microvasculature after 5 days in *ex vivo* culture. Bioprinted 4T1 murine breast cancer cells onto wild-type mesometrium tissues were cultured *ex vivo* for 5 days. Tissues with cells were fixed in methanol and labeled against PECAM and E-cadherin to identify endothelial cells lining the microvasculature and cancer cells, respectively. After 5 days, the microvasculature is angiogenic indicative by the sprouts (arrows). Scale bars = $100 \ \mu m$.

Fig. 7. The presence of breast cancer cells has an effect on the appearance of angiogenic microvasculature but not on the number of sprouts or segments. Bioprinted 4T1 murine breast cancer cells onto wild-type mesometrium tissues (D-F) and sham control excluding cancer cells (A-C) were cultured *ex vivo* for 5 days. Tissues with cells were fixed in methanol and labeled against PECAM to identified endothelial cells lining the microvasculature. Both groups were angiogenic indicative of the sprouts (arrows), and had the presence of vascular islands, disconnected segments (*). After 5 days in culture, the number of sprouts (G), segments (H), and vascular islands (I) were quantified for the sham control (white circle symbol) and the bioprinted cancer cells (black circle symbol). Data is shown as the mean \pm SEM and * represents p < 0.05, n = 7. Scale bars = 100 μm.

Figure 1

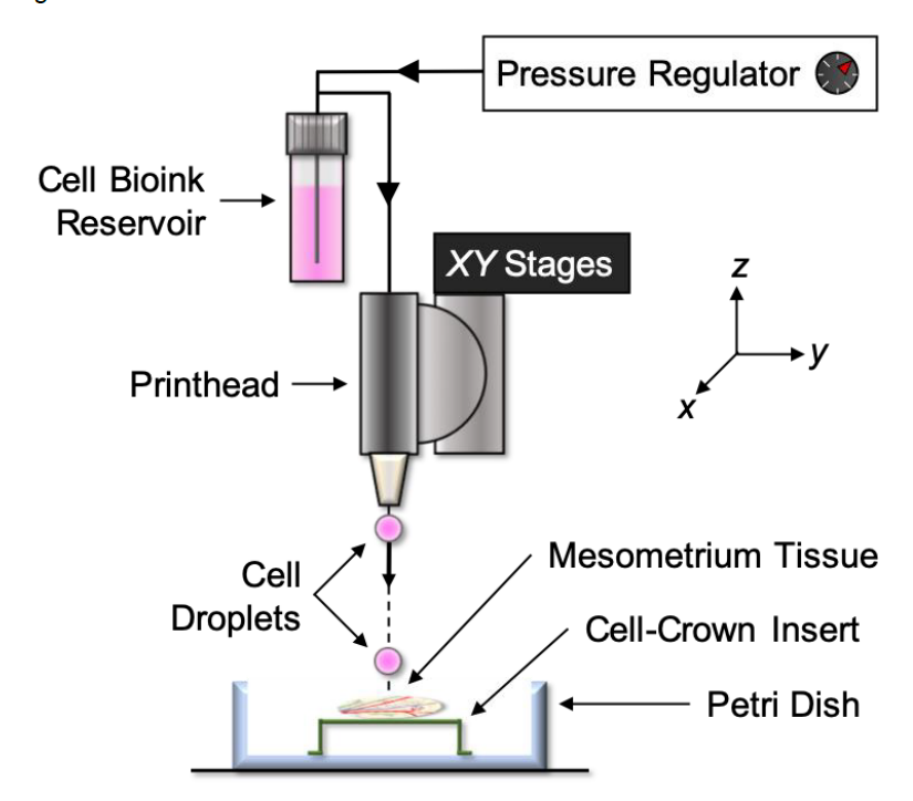


Figure 2

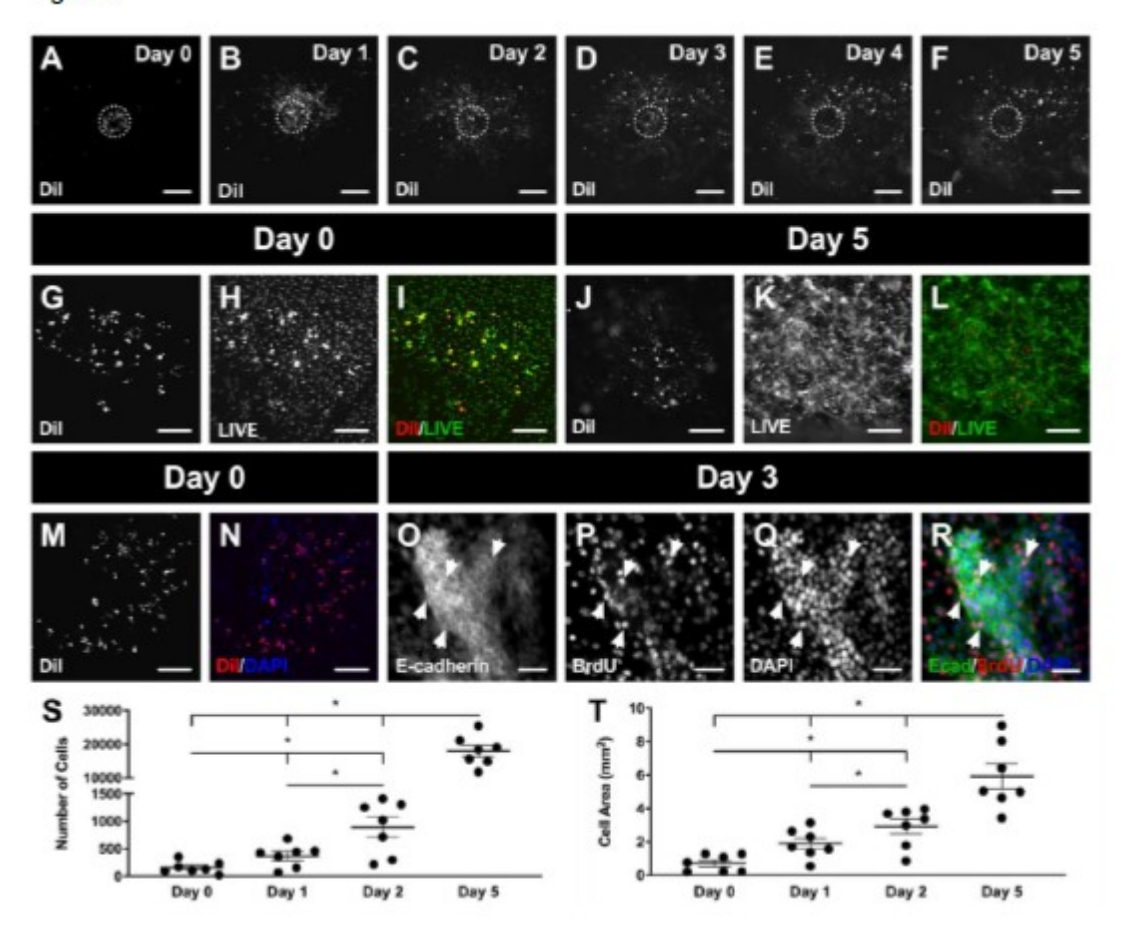


Figure 3

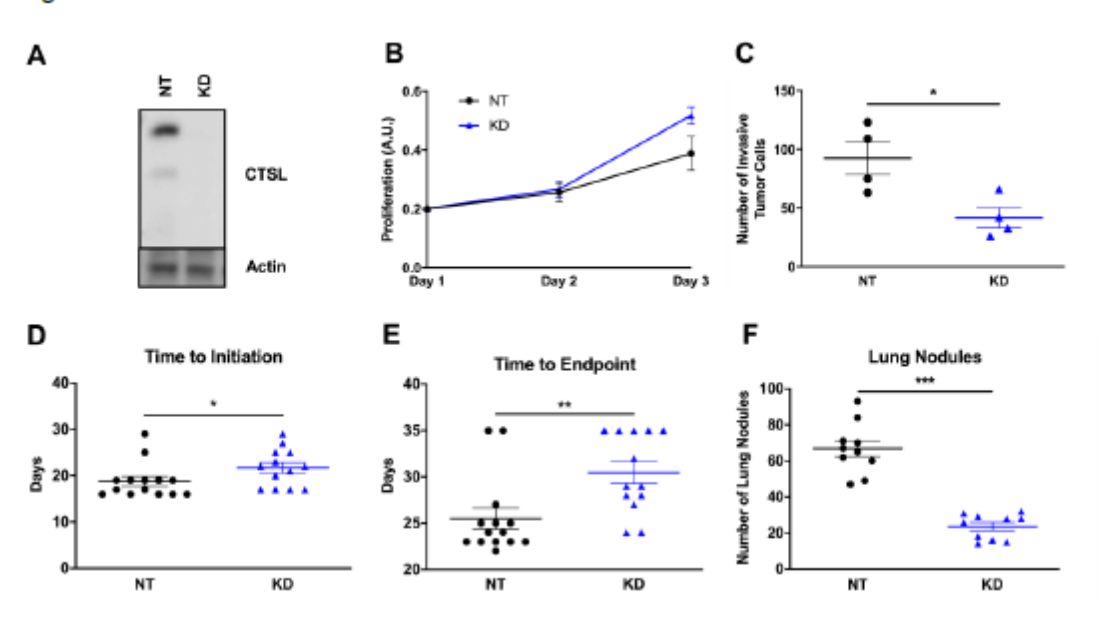


Figure 4

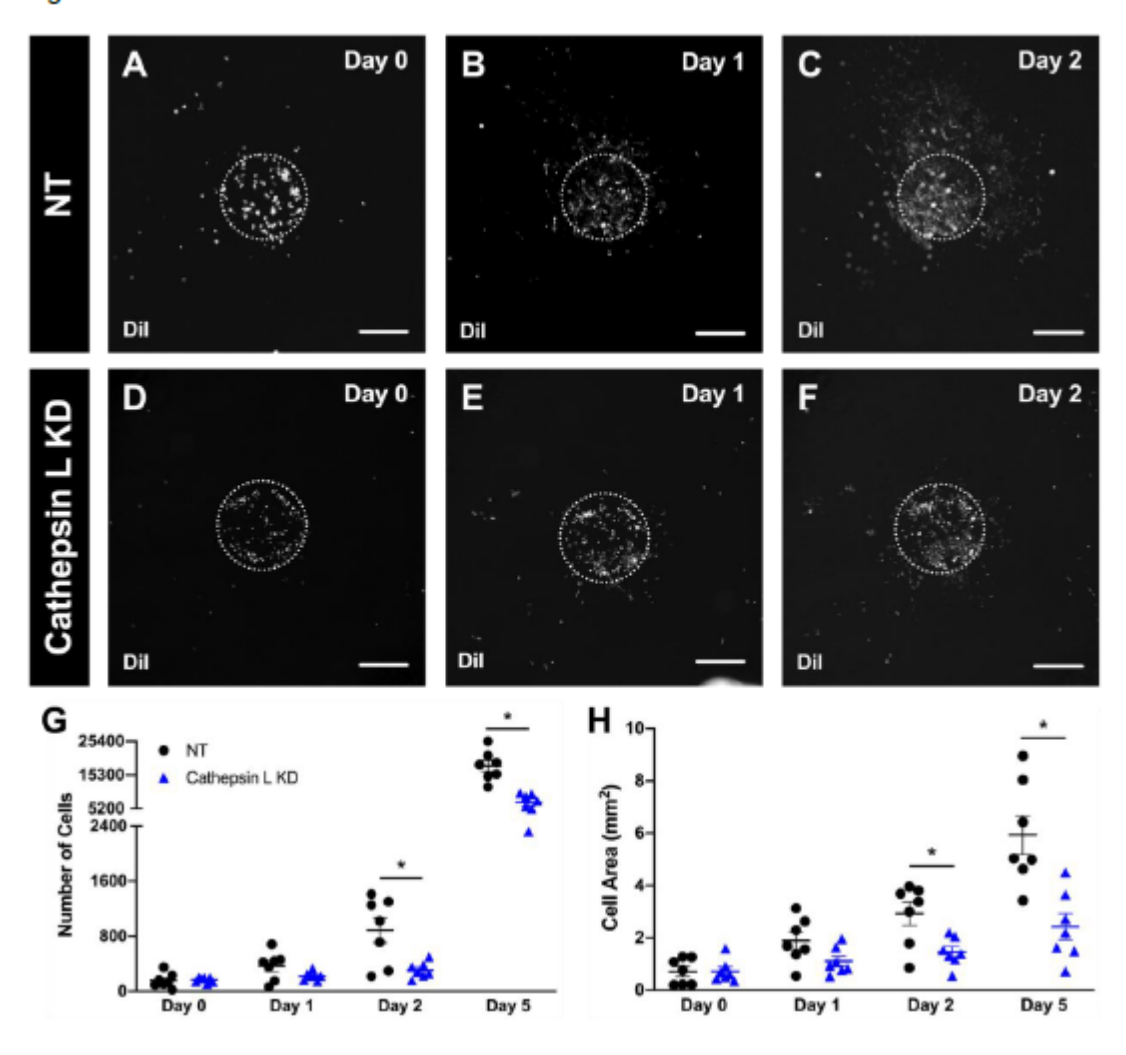


Figure 5

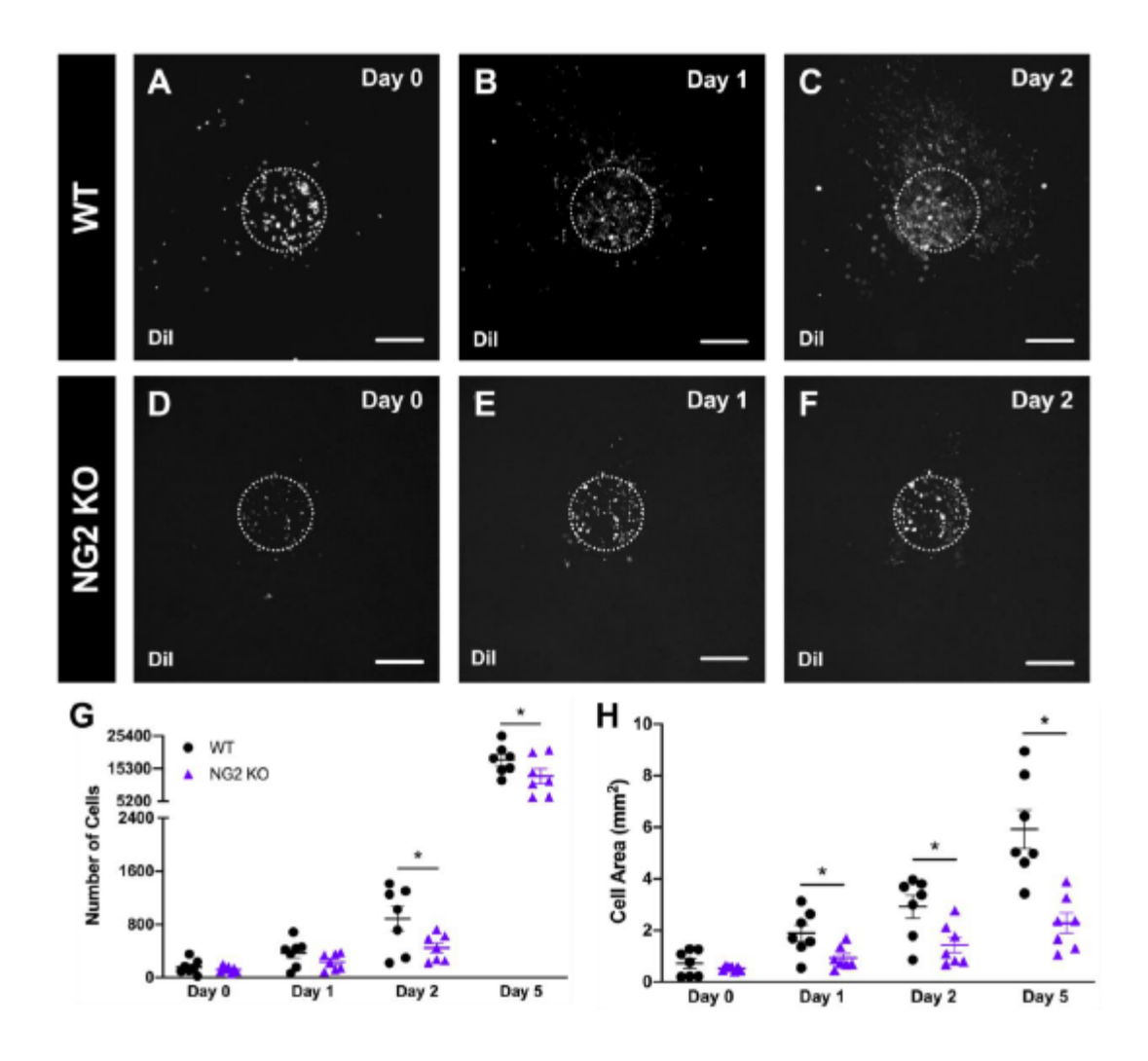


Figure 6

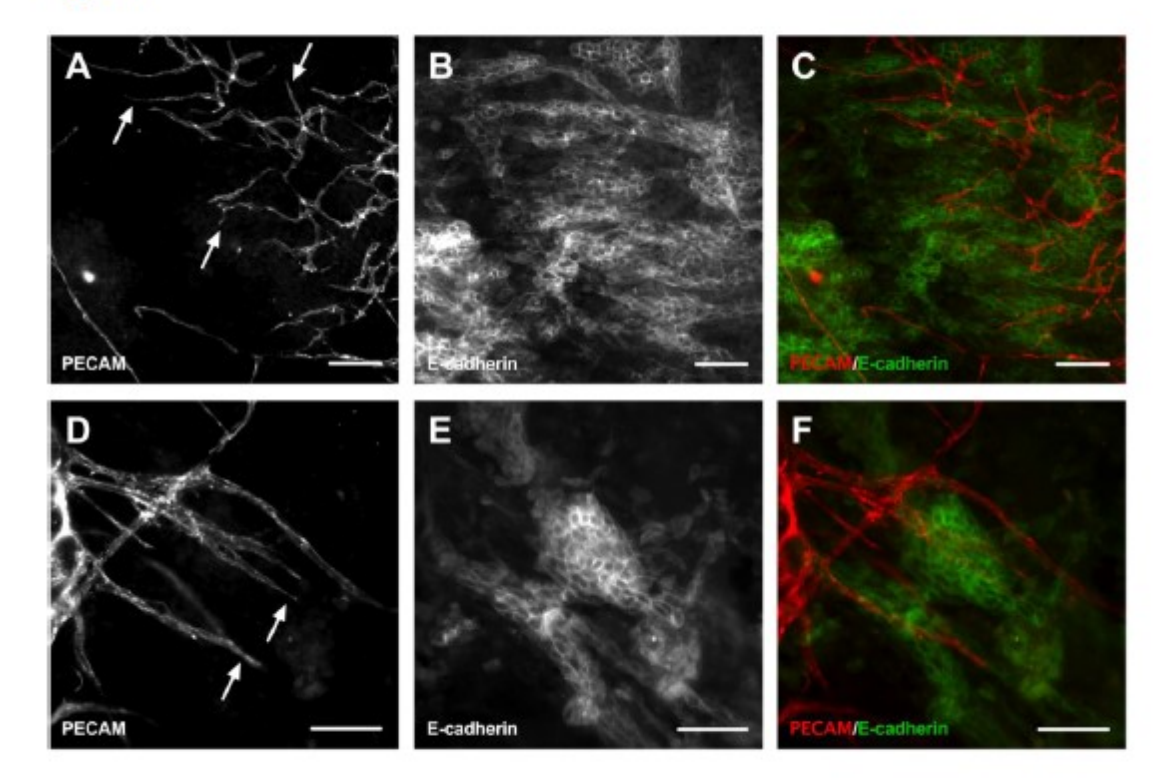


Figure 7

